Polarized x-ray-absorption spectroscopy of the uranyl ion: Comparison of experiment and theory

E. A. Hudson, P. G. Allen, and L. J. Terminello
Glenn T. Seaborg Institute for Transactinium Science, Lawrence Livermore National Laboratory, University of California, Livermore, California 94551

M. A. Denecke and T. Reich
Institut für Radiochemie, Forschungszentrum Rossendorf, Postfach 510119, D-01314 Dresden, Germany
(Received 16 October 1995; revised manuscript received 11 January 1996)

The x-ray linear dichroism of the uranyl ion (UO_2^{2+}) in uranium L_3-edge extended x-ray-absorption fine structure (EXAFS), and L_1- and L_3-edge x-ray-absorption near-edge structure (XANES), has been investigated both by experiment and theory. A striking polarization dependence is observed in the experimental XANES and EXAFS for an oriented single crystal of uranyl acetate dihydrate [$UO_2(CH_3CO_2)_2 \cdot 2H_2O$], with the x-ray polarization vector aligned either parallel or perpendicular to the bond axis of the linear uranyl cation (O-U-O). Single-crystal results are compared to experimental spectra for a polycrystalline uranyl acetate sample and to calculations using the *ab initio* multiple-scattering (MS) code FEFF 6. Theoretical XANES spectra for uranyl fluoride (UO_2F_2) reproduce all the features of the measured uranyl acetate spectra. By identifying scattering paths which contribute to individual features in the calculated spectrum, a detailed understanding of the L_1-edge XANES is obtained. MS paths within the uranyl cation have a notable influence upon the XANES. The measured L_3-edge EXAFS is also influenced by MS, especially when the x-ray polarization is parallel to the uranyl species. These MS contributions are extracted from the total EXAFS and compared to calculations. The best agreement with the isolated MS signal is obtained by using nonoverlapped muffin-tin spheres in the FEFF 6 calculation. This contrasts the L_1-edge XANES calculations, in which overlapping was required for the best agreement with experiment. [S0163-1829(96)00125-7]

I. INTRODUCTION

For aqueous solutions, in the presence of air, uranium is nearly always found as the uranyl oxocation, $U^{VI}O_2^{2+}$. This species consists of a formally +6 uranium atom tightly bound to two oxygen atoms in a symmetric linear structure (O-U-O). The uranyl cation has a complicated solution chemistry, with the formation of oligomers and strong complexation by hydroxide and carbonate among the many possibilities.[1] However, in all these complexes the O-U-O structure of the uranyl cation is preserved. This species is also present in a large number of solids, with a great variety of counter ions.[2] Analogous linear actinyl cations exist for several other actinides, specifically neptunium, plutonium, and americium.[3]

Because the uranyl cation is prevalent and exhibits unusually strong covalent bonding, it has been the focus of considerable study.[4] X-ray-absorption spectroscopy (XAS), in particular, has been used to characterize uranyl speciation and structure.[5–7] Growing interest in the XAS of actinides reflects the ability of this technique to study dilute quantities of hazardous materials in systems with environmental relevance, such as aqueous complexes with organic chelating agents[5,6] or mineral-surface sorption complexes.[8–12] For uranium, the L_3 absorption edge at $\approx$17.2 keV is perhaps the most useful, allowing the straightforward measurement of extended x-ray-absorption fine structure (EXAFS), and providing oxidation-state and structural information in the x-ray-absorption near-edge structure (XANES).[13–15] However, interpretation of the L_3-edge EXAFS and XANES for the uranyl cation may be complicated by the contributions of photoelectron multiple-scattering (MS) paths.

In order to better understand MS effects, and to establish a more fundamental basis for XAS studies of uranium, the x-ray linear dichroism of uranyl L_3-edge EXAFS and XANES has been investigated both by experiment and theory. This effect has also been studied for the L_1-edge XANES, which samples different final states than the L_3 edge. A striking polarization dependence is observed in the experimental XANES and EXAFS for an oriented single crystal of uranyl acetate dihydrate, depending upon the alignment of the x-ray polarization vector either parallel or perpendicular to the uranyl bond axis. The polarized XANES spectra are very similar to those measured by Templeton and Templeton for single-crystal rubidium uranyl nitrate.[16] The large XANES polarization dependence could be utilized to experimentally determine the orientation of the linear uranyl species, e.g., to measure the orientation of adsorbed uranyl relative to a layered mineral substrate.

The single-crystal experimental results are compared to measured spectra for a polycrystalline uranyl acetate sample and to calculations for uranyl fluoride using the *ab initio* MS code FEFF 6.[17] The theoretical XANES spectra reproduce all the features of the measured spectra. By identifying the photoelectron scattering paths which contribute to individual features in the calculated spectrum, a detailed understanding of the L_1-edge XANES is obtained. MS paths within the uranyl cation are shown to have a notable influence upon the XANES.

The measured L_3-edge EXAFS also shows the influence of MS, especially when the x-ray polarization is parallel to the uranyl species. The implication is that the analysis of

uranyl EXAFS, in general, should include MS contributions to obtain reliable structural information for atoms at distances >2.5 Å. The MS contributions can be extracted from the total EXAFS, allowing a detailed comparison to theory. The best agreement with the isolated MS signal is obtained by using nonoverlapped muffin-tin spheres in the FEFF 6 calculation. This contrasts the L_1-edge XANES calculations, in which overlapping was required for the best agreement with experiment.

II. EXPERIMENTAL PROCEDURES AND DATA REDUCTION

Uranyl acetate dihydrate [$UO_2(CH_3CO_2)_2 \cdot 2H_2O$, or UO_2Ac_2] possesses an orthorhombic crystal structure, with the linear uranyl cations aligned parallel (within 1°) to the *a* axis.[18] Single crystals were grown by slow evaporation from a solution of ≈ 0.8 M UO_2Ac_2 (reagant grade) and ≈ 0.1 M acetic acid (electronic grade). A well-formed rectangular prism measuring ≈ 0.6 mm$\times\approx 0.7$ mm$\times\approx 0.2$ mm was selected for XAS. The smallest dimension of this crystal, in particular, has a rather uniform thickness. The orientation of the crystal lattice *a* axis was determined by visible linear dichroism. Due to the symmetry of the broad uranyl optical absorption transition, peaked at ≈ 415 nm, the distinctive yellow color of the crystal is not observed for linearly polarized light with the electric-field vector **E** parallel to the uranyl bond axis.[4] The *a* axis was found to be parallel to the ≈ 0.7 mm dimension. The *b* axis was assumed to be parallel to the ≈ 0.2 mm dimension. This corresponds to the largest crystal face presenting only dangling hydrogen bonds, easily satisfied by hydration, and thus possessing the lowest free energy. This choice is also consistent with the generalized Law of Bravais.[19] A 13 mm diameter powdered polycrystalline UO_2Ac_2 sample was also prepared, with a thickness of 1 mm, using boron nitride as a buffer material to adjust the L_3 absorption edge jump to approximately unity, the optimal value for transmission XAS.

XAS measurements were performed in transmission mode using Si(220) double-crystal monochromators on wiggler beamlines 4-1 and 4-3 at the Stanford Synchrotron Radiation Laboratory (SSRL). The single-crystal XANES measurements were reproduced using a similar monochromator on bending magnet beamline 2-3 at SSRL. The beam size was cropped after the monochromator exit slit to 0.5 mm$\times$0.5 mm for the single-crystal sample and 10 mm$\times$0.5 mm for the polycrystalline sample. Argon-filled ionization chambers were used to monitor the incident and transmitted x-ray flux, as well as flux transmitted by a uranyl nitrate hexahydrate energy calibration standard placed downstream from the sample. Spectra were measured for the single crystal oriented with the *b* axis parallel to the x-ray beam and the *a* axis either horizontal or vertical ($\pm 2°$). Approximately 98% of the synchrotron radiation is plane polarized with **E** horizontal, so these orientations correspond to the electric vector parallel or perpendicular to the uranyl bond axis, respectively. These data sets will be referred to as ''parallel'' and ''perpendicular.''

The energy scales for the XANES spectra were calibrated as follows. The L_3-edge white line maximum was assumed to be at photon energy 17 175 eV for the uranyl nitrate reference.[13] In the absence of a reliable calibration energy for the uranyl nitrate L_1 edge, the maximum of the largest resonance was assumed to be 21 835 eV, which makes the edge inflection point roughly equal to the calculated ionization potential for α-uranium metal.[20] The L_1-edge XANES spectra were normalized by removing a background based on a fit to the pre-edge region and then defining the absorption coefficient to be unity at 21 870 eV. The L_3-edge spectra were similarly normalized at 17 231 eV. The normalization factors were 0.965, 0.970, and 0.907 for the parallel, perpendicular, and polycrystalline L_3 spectra, respectively; close to the optimal edge jump of unity. The nearly equal values for the two single-crystal spectra indicate a uniform effective sample thickness for these measurements. This shows that the rather small crystal was well-positioned in the beam for both orientations.

EXAFS data reduction followed standard procedures, using the EXAFSPAK software package.[21] The photon energy scale of each scan was calibrated by assuming a 17 171 eV inflection point for the L_3-edge jump of the uranyl nitrate reference. The ionization threshold energy E_0 was assumed to be 17 180 eV, a value which allows good fits to the data without adjusting the theoretical E_0 values, with one exception as described below. Fits and Fourier transforms utilized k^3-weighted χ data over the range $k=2.5$–10.5 Å^{-1}. The data fitting is discussed in detail below.

III. THEORETICAL CALCULATIONS

XANES and EXAFS calculations were performed using the general purpose XAS code FEFF, developed by Mustre de Leon *et al.*[22] This theoretical approach models the photoelectron final state by an *ab initio* curved-wave MS calculation, using a complex energy-dependent exchange-correlation self-energy within a muffin-tin potential. The latest version, FEFF 6, computes the absorption coefficient $\mu(E)$ by combining the fine structure $\chi(k)$ with an atomic absorption background $\mu_0(E)$, using a well-defined ionization potential E_0.[17] The photoelectron wave number k is related to the photon energy E by $k^2 \propto [E-E_0]$. FEFF 6 also allows the calculation of XAS spectra with polarized x rays.

Recent calculations used FEFF 6 to model unpolarized uranium L_3-edge XANES for a variety of uranium compounds.[15] Good agreement between theory and experiment indicated that this approach is adequate for high-Z elements. Results for uranyl fluoride, UO_2F_2, showed that successful modeling of the L_3 above-edge resonance required the use of overlapped muffin-tin spheres, which apparently better simulate the anisotropic uranyl structure.[15] This resonance, which lies ≈ 10 eV above the white line, was shown to originate from MS paths within the linear uranyl cation. These results demonstrated the value of a path analysis, i.e., where the set of scattering paths used in the XANES calculation is varied, to identify correlations between individual spectral features and specific paths. A similar approach is used here to interpret the L_1-edge XANES of UO_2Ac_2. Additional comparisons are presented to demonstrate the influence of the degree of muffin-tin overlap upon both XANES and EXAFS.

Although the crystal structure and atomic arrangement of UO_2Ac_2 has been determined by single-crystal x-ray

diffraction,[18] the positions of the hydrogen atoms are not known. Even if approximate positions were assumed for FEFF 6 calculations, the use of a muffin-tin potential to model oxygen or carbon bound to hydrogen may be inaccurate due to the short bond lengths and highly directional bonds. These shortcomings of the muffin-tin potential can also introduce convergence problems in the phase shift calculations, effectively limiting the choice of overlap parameters used to construct the potential. Therefore experimental results for UO_2Ac_2 are compared here to calculations for UO_2F_2. This approach is justified for several reasons. Previously measured uranyl L_3-edge XANES spectra show little or no dependence on the counter-ions,[13–15] and the polarized L_1- and L_3-edge XANES spectra measured here for UO_2Ac_2 are quite similar to the results of Templeton and Templeton for $RbUO_2(NO_3)_3$.[16] For EXAFS purposes, scattering phase shifts and amplitudes depend only weakly on atomic number. Chemical effects on these parameters may be significant, but the chemical environment of uranyl axial oxygens and equatorial ligand atoms should be fairly similar in UO_2F_2 and UO_2Ac_2. Although UO_2F_2 has an equatorial coordination number of six, while the value for UO_2Ac_2 is five, the two compounds have similar axial and equatorial bond distances.[18,23]

The single-scattering (SS) XAS fine structure is given by

$$\chi(k)=S_0^2C(k)\sum_i \frac{N_iF_i^{\rm eff}(k,R_i)}{kR^2}\exp\left(\frac{-2R_i}{\lambda(k)}\right)\exp(-2\sigma_i^2k^2) \times\sin[2kR_i+\phi_i(k,R_i)+\phi_c(k)], \quad (1)$$

where the summation is over each shell i with N_i atoms at distance R_i from the absorbing atom. This expression includes factors for intrinsic core-hole relaxation losses S_0^2, extrinsic central-atom losses C, effective backscattering magnitude $F_i^{\rm eff}$, photoelectron mean free path λ, Debye-Waller (DW) broadening (using the DW factor σ_i^2), and the oscillatory k dependence (with atomic phase shifts ϕ).[22] Note that the λ used here represents the decay of photoelectron wave-function amplitude and is thus twice the mean free path given by a more widely used definition which refers to decay of electron intensity. FEFF 6 models only dipole transitions, with the further restriction of the $l+1$ approximation. For the L_1 edge, this assumes p-symmetry final states, and is exact within the dipole approximation, but for the L_3 edge it assumes only d final states. Besides ignoring transitions to isotropic s final states, this simplification fails to consider a term arising from interference between s and d final states.[24,25] The sd interference averages to zero in unpolarized spectra but may make substantial contributions to polarized spectra.[26] The absence of sd interference in the calculations may explain some discrepancies in the EXAFS results discussed below.

For the analysis of the L_3-edge EXAFS, the polarization-dependent part of the curved-wave corrections to the backscattering amplitude and phase, F_i and ϕ_i,[27,28] are left out. Test calculations showed these effects to be small above the L_3 edge for the SS paths, especially for $k>3.5$ Å^{-1}, and very small for the MS paths. Polarization effects[24] are then easily incorporated into Eq. (1) by introducing effective coordination numbers

$$N_i^e=\tfrac{1}{2}N_i(1+3\cos^2\theta_i), \quad (2)$$

where the index i now identifies shells with unique R_i and θ_i. The angle θ_i is defined as the angle between the electric field vector $\mathbf{E}$ of the x ray and the vector $\mathbf{R}_i$ from the absorbing atom to the scatterer. Note that the fits to the measured EXAFS, described below, combine calculated UO_2F_2 scattering parameters with effective coordination numbers based on the UO_2Ac_2 atomic positions.

Multiple-scattering paths can be included in Eq. (1) as additional terms in the sum. For the linear, centrosymmetric MS paths considered here, the angular dependence given above for N_i^e is valid. Atomic disorder is represented in Eq. (1) by the DW factor σ_i^2, which is the relative mean-square displacement along $\mathbf{R}_i$.[29] This can be generalized for MS (Ref. 30) by summing over each leg j of the SS or MS path i

$$\sigma_i^2=\frac{1}{4}\left\langle\left[\sum_j \sigma_j\right]^2\right\rangle. \quad (3)$$

The MS DW factors can be related to SS DW factors using known or assumed correlations in the averaging of the individual terms in the squared sum. There are two specific cases relevant to the three MS paths which are important here: Case (A) $U\rightarrow O_1\rightarrow U\rightarrow O_1\rightarrow U$ within the same axial U-O bond (path MS2), and Case (B) $U\rightarrow O_1\rightarrow U\rightarrow O_2\rightarrow U$ and $U\rightarrow O_1\rightarrow O_2\rightarrow U$ within the linear O-U-O chain (paths MS1 and MS3, respectively). For case (A), clearly the bond distance is perfectly correlated to itself, so $\sigma_{\rm ms}^2=4\sigma_{\rm ss}^2$, where $\sigma_{\rm ss}^2$ applies to the axial U-O SS. For case (B), ignoring curved-wave and bending-motion effects, $\sigma_{\rm ms}^2=q\sigma_{\rm ss}^2$, where q can vary between 0 and 4, corresponding to the two extremes of symmetric- and asymmetric-stretch vibrational modes, but q must be equal for MS1 and MS3. For uranyl, where the large central atom mass causes the amplitudes of these two stretching modes to be roughly equal, q should be close to 2, the value for uncorrelated U-O_1 and U-O_2 bond distances.

IV. X-RAY-ABSORPTION NEAR-EDGE STRUCTURE

A. Experimental results

Figure 1 shows the measured L_1 and L_3 XANES of UO_2Ac_2, for a single crystal with polarization either parallel or perpendicular to the uranyl bond axis, and for a randomly oriented polycrystalline sample (i.e., equivalent to an unpolarized measurement). The striking variations observed here agree with those of the polarized spectra measured by Templeton and Templeton for rubidium uranyl nitrate.[16] This similarity suggests that the observed spectral features arise primarily within the uranyl species, perhaps with contributions from the surrounding shell of equatorial oxygen atoms. The polycrystalline spectra are close to the average (not shown) of the perpendicular and parallel spectra, with weighting factors $\frac{2}{3}$ and $\frac{1}{3}$, respectively. This is expected for a dichroic crystal,[25] i.e., if the rather low symmetry of the equatorial coordination shell around uranyl in UO_2Ac_2 is unimportant. Note, in particular, that peak 1, emphasized in the parallel L_1 spectrum, is observed as a shoulder in the polycrystalline L_1 spectrum.

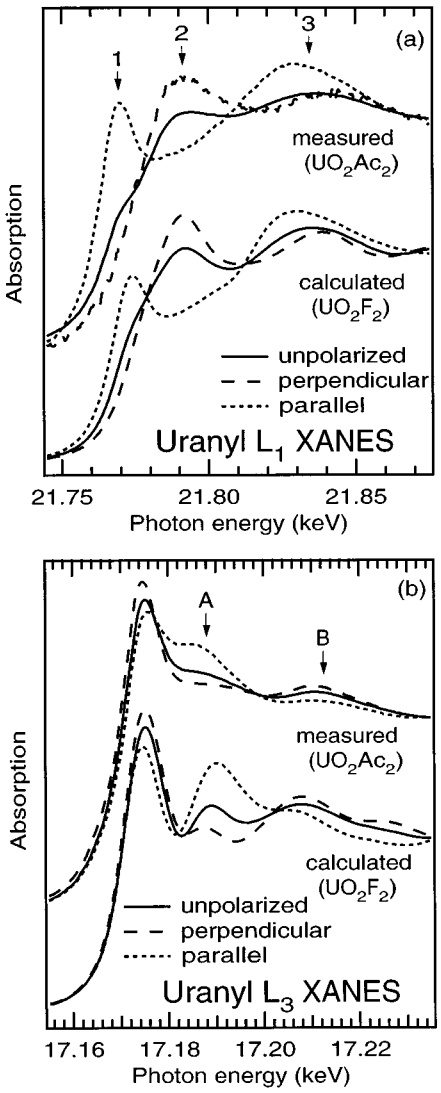

FIG. 1. Polarization dependence of uranyl (a) L_1-edge and (b) L_3-edge XANES. Experimental spectra were measured using UO_2Ac_2 and theoretical spectra were calculated using UO_2F_2. The solid lines represent either a measured polycrystalline sample or an unpolarized calculation. The long- and short-dashed lines represent x-ray polarization perpendicular and parallel to the uranyl bond axis, respectively.

The polarization dependence of the experimental L_1 XANES, in Fig. 1(a), allows a rough assignment of features in the polycrystalline spectra. Peak 1 and the lower-energy part of peak 3, which are enhanced in the parallel spectrum, arise mainly from scattering off the axial uranyl oxygens. Peak 2 and the higher-energy part of peak 3, enhanced in the perpendicular spectrum, arise mainly from scattering off equatorial oxygen atoms, or perhaps more distant atoms in the equatorial plane. Alternatively, if the uranyl is treated as an isolated linear molecule, the $2s$ core state has σ_g symmetry, and dipole selection or rules dictate that the parallel and perpendicular XANES sample σ_u and π_u final states, respectively. In either case, a characterization is obtained for the individual spectral features of the polycrystalline XANES.

B. Theoretical results

The results of FEFF 6 calculations for UO_2F_2 are also plotted in Fig. 1. The calculations are based on a 12-shell cluster with 83 atoms and a radius of 6.5 Å, assuming the atomic positions determined by neutron diffraction.[23] Calculated energies are shifted $+23$ ($+20$) eV for the L_1 (L_3) edge to give the best agreement with experiment. To simulate the effects of experimental resolution, the L_1 (L_3) spectra are convoluted with a Gaussian function of 6 eV (5 eV) width [full width at half maximum (FWHM)]. Note that the calculations also include the 14.0 eV (7.4 eV) Lorentzian natural linewidth (FWHM) for the $2s$ ($2p_{3/2}$) core hole.[31] The calculated XANES are in good agreement with the experimental results, reproducing the polarization dependence of all individual spectral features. In particular, the intensity variation of the L_3 above-edge resonance, peak A, is qualitatively modeled by the calculations, further supporting the previous assignment of this feature to a MS resonance.[14,15]

The agreement between calculated and measured XANES is notably better for the L_1 edge than for the L_3 edge. There are several possible explanations: (1) This result may reflect the $l+1$ approximation used in the calculation, which is more accurate for the L_1 edge, as discussed in Sec. III. Note that similar faults in the calculated L_3-edge XANES are observed for the polarized *and* unpolarized spectra, i.e., peak A is too high in energy and too narrow, and peak B is too low in energy. These polarization-independent errors cannot arise from sd interference, but could be caused by pure $p \rightarrow s$ transitions. However the $p \rightarrow s$ transitions may be too weak to explain the magnitude of the disagreement.[32] (2) Another possibility is that the d final states are not modeled as successfully as the p states, perhaps because the d states are more sensitive to inaccuracies of the potential. (3) The greater core-hole lifetime for the L_3 edge allows contributions from longer scattering paths, which are generally more difficult to model. In fact, several paths to atoms outside a U-O_2-F_6 two-shell cluster were found to be significant for the L_3 XANES in Ref. 15, whereas the path analysis below indicates that the L_1 XANES arises only from paths within such a cluster.

1. Path analysis

Figure 2 shows the results of a path analysis for the L_1 XANES, i.e., a comparison of results from calculations based on limited sets of scattering paths. The experimental UO_2Ac_2 spectra from Fig. 1(a) are also plotted for comparison. Figure 2(b) presents the path analysis for the unpolarized case. The full calculation, which includes 21 unique scattering paths, is reproduced from Fig. 1(a), and the curves below are based on subsets of these paths. A curve nearly identical to the full calculation is obtained using single-scattering (SS) paths to equatorial (second-shell) fluorine atoms along with SS and MS paths to the axial oxygens of the uranyl species. However a calculation based only on the axial SS and MS paths is rather different, still showing the lower-energy part of peak 3 and the shoulder for peak 1, but missing most of the intensity for peak 2. A similar result, with a weaker shoulder for peak 1, is obtained using only the axial SS path. The final calculation shown in Fig. 2(b), based on equatorial SS, shows only peak 2 and the higher-energy

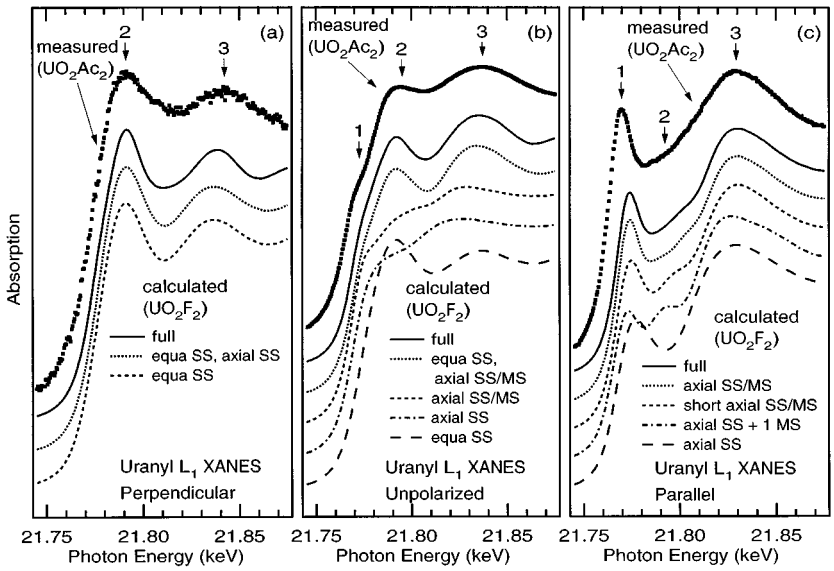

FIG. 2. Scattering path analysis for uranyl L_1-edge XANES: (a) Polarization perpendicular to uranyl bond axis, (b) Unpolarized, (c) Polarization parallel to uranyl bond axis. The curves, as labeled, are the results of calculations using various subsets of the ''full'' path sets. See text for details.

part of peak 3. From this comparison it is evident that peak 1 and the lower-energy part of peak 3 arise from scattering from the axial oxygens, while peak 2 and the higher-energy part of peak 3 arise from scattering off the equatorial atoms. These conclusions, obtained from the *unpolarized* path analysis, are the same as those determined in Sec. IV A from the polarization dependence of the experimental spectra.

Figure 2(a) shows a path analysis for perpendicular polarization. The full calculation (14 paths) is very similar to results based on equatorial SS and axial SS (two shells) or equatorial SS (second shell only). This indicates that the perpendicular L_1 XANES results only from SS paths to the equatorial atoms. Figure 2(c) presents a path analysis for parallel polarization. The full calculation (12 paths) is reproduced using only SS and MS paths within the uranyl species. If MS paths longer than ≈ 7 Å (twice the SS path length) are excluded, the result (labeled ''short axial SS/MS'') is nearly the same, except peak 1 broadens somewhat, becoming less similar to experiment. Calculations based either on axial SS and the strongest MS path, or on axial SS alone, show considerable differences, and a much poorer agreement with experiment. These results clearly indicate a MS origin for peak 1, as well as for the residual intensity in the region of peak 2, observed for parallel polarization. Peak 1 is best modeled by including longer MS paths, but is reasonably well modeled using the three shortest MS paths, which are also discussed below in reference to the L_3-edge EXAFS. Note that the energy of peak 1 is calculated ≈ 5 eV too high, relative to the other peaks.

2. Overlap analysis

Muffin-tin overlap is a computational method, wherein the radii of the muffin-tin spheres, which define the volumes used to determine scattering parameters for each atom, are increased such that adjacent spheres overlap. The calculation then becomes a little inconsistent, because each atom is still treated independently, even though electron wave functions from neighboring atoms actually extend into the sphere. Overlapping is commonly introduced into a muffin-tin potential to better model anisotropic bonding, for which significant charge density may lie outside the nonoverlapped radii.[33] All of the calculations presented above are based on a potential in which the muffin-tin spheres were overlapped using the method of Norman.[34] The degree of overlap is, in fact, an influential parameter for these XANES calculations. Figure 3 presents a comparison of L_1 XANES calculations covering a range of 0–1.25 in the overlap parameter u where $r^i = r^i_{mt} + u(r^i_n - r^i_{mt})$ is the radius used in the calculation for atom i, based on r^i_{mt}, the nonoverlapped radius, and r^j_n, the Norman radius. For the absorbing uranium atom, $r_{mt} = 1.09$ Å and $r_n = 1.50$ Å . In the extreme of $u = 1.25$, the radius used for this atom becomes 1.60 Å , which is nearly equal to the 1.74 Å U-O bond distance. The potential obtained using such a large degree of overlap may be unphysical but the calculation is nevertheless included here as a limiting case. Overall, the calculations with $u = 1.00$, i.e., using the Norman radius, give the best agreement with experiment. A similar result was previously obtained for the L_3 XANES of uranyl fluoride.[15]

Figure 3(a) compares the overlap results for perpendicular polarization. Peak 2 shows the most variation, with the best match to experimental relative intensity for $u = 1.00$ and to experimental width for $u = 0.75$. The overlap dependence in this case arises almost entirely from variations in the atomic absorption background μ_0 (not shown). For the parallel case, shown in Fig. 3(c), the calculations use the same μ_0 as for the perpendicular case, but the overlap dependence arises mainly from changes in the fine structure χ (not shown). Peaks 1 and 3 shift to their lowest energy values for $u = 1.00$, and the width of peak 1 is minimized, to give the best agreement with the measured parallel spectrum. The width of peak 3 is better modeled by $u = 0.75$ or 0.50. The unpolarized case, shown in Fig. 3(b), shows the combined effects of the polarized results; for $u = 1.00$, peaks 1 and 3 shift to their lowest energies, and the relative intensity of peak 2 increases, giving the best match to experiment. Thus overlapping with r^i equal to (or slightly less than) the Norman radius has two beneficial effects, (1) it improves the modeling of scattering for resonances within the linear ura-

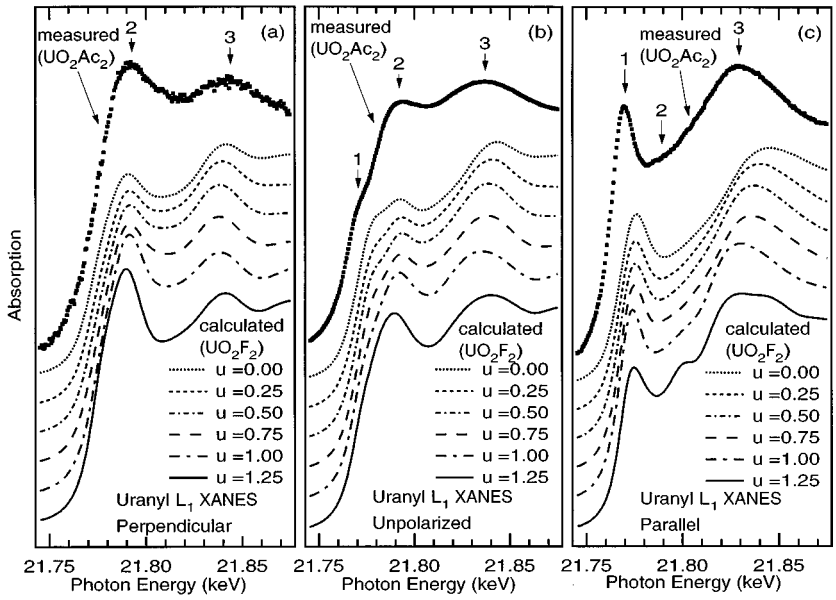

FIG. 3. Muffin-tin overlap analysis for uranyl L_1-edge XANES: (a) Polarization perpendicular to uranyl bond axis, (b) Unpolarized, (c) Polarization parallel to uranyl bond axis. The curves, as labeled, are the results of calculations using a range of values for u, the muffin-tin overlap parameter. See text for details.

nyl group, (2) it optimizes the atomic background μ_0 in the region of peak 2.

V. EXTENDED X-RAY-ABSORPTION FINE STRUCTURE

A. Experimental results

The measured L_3-edge EXAFS for UO_2Ac_2 are shown in Fig. 4. A large dependence upon polarization is seen for $k^3\chi(k)$, in Fig. 4(a), which is more easily interpreted by examining the Fourier transforms (FT's), in Fig. 4(b). These each exhibit two major peaks, at $R+\Delta \approx 1.3$ and 1.9 Å, which correspond to the uranyl axial oxygen shell and the equatorial oxygen shell, respectively. As expected, the axial peak is maximized for parallel polarization and minimized for perpendicular polarization, while the opposite trend is observed for the equatorial peak. However, contrary to expectations, the axial peak is barely diminished in the perpendicular FT, relative to the polycrystalline FT. A third peak is observed at $R+\Delta \approx 2.8$ Å, which is most intense for parallel polarization. This polarization dependence suggests that the peak arises from MS within the linear uranyl group, rather than SS to another shell, because there are no neighboring atoms at the appropriate distance in the direction parallel to the uranyl axis. Note that the phase-shifted path length for this MS peak is about twice that of the axial SS peak.

B. Results of EXAFS fitting

Figure 4 also plots the results of least-squares fits to $k^3\chi(k)$, and quantitative results from the fits are listed in Table I. A study of UO_2Ac_2 by x-ray diffraction (XRD) located three types of oxygen atoms in the uranyl equatorial shell: two from monodentate acetate ligands, two from a bidentate acetate, and one from water, with the distinct bond distances listed in Table I.[18] However, to simplify the EXAFS data analysis a uniform equatorial shell with five atoms was assumed. Likewise, a very small asymmetry in the axial oxygen bond distances, also determined by XRD, was ignored here. For the polarized EXAFS, the effective coordination numbers N_i^e in Table I were calculated using the UO_2Ac_2 XRD structure and Eq. (2). The assumed orientation of the lattice c axis, mentioned in Sec. II, influences the value of N^e for the equatorial shell (by $<10\%$). However the quantitative fit results are only slightly dependent upon this assumption, and all of the conclusions below remain valid if alternative orientations of the c axis are assumed.

As mentioned in Sec. III, the scattering parameters used in the fits were calculated for UO_2F_2. A single MS path, designated MS1, was included in the fit. The DW factor for the path MS1 was held proportional to the DW factor for the axial SS path, using $q=2$ (see Sec. III). The effective bond distance R_{MS1} for MS1 was held at twice the axial SS bond distance, R_{SS1}, and N^e_{MS1} was equal to N^e_{SS1}. Thus the inclusion of the MS path did not introduce any adjustable parameters. The automatic muffin-tin overlap feature of FEFF 6 was used, equivalent to $u=0.7$; alternative fits using $u=0.0$ yielded slightly different quantitative results but support all the following conclusions. This consideration of overlap is essential in light of the results in Sec. V C below.

The derived bond distances for the polycrystalline data, listed in Table I, agree rather well with the averaged XRD values, and the DW values for this data set are comparable to those found in other uranyl EXAFS studies.[5,6,8,9,35] The successful fitting of the polycrystalline data indicates that the use of UO_2F_2 scattering parameters and a simplified geometry is valid here. Further examination of the fit parameters in Table I reveals several notable results, which reflect discernible trends in the experimental FT's. The bond distances and DW factors show some variation between the different data sets. In particular, the uranyl axial bond distance R^{SS1} shows a decrease (-0.05 Å) for the perpendicular case and a slight increase ($+0.02$ Å) for the parallel case. Also, the DW factor obtained for this shell is very small for the perpendicular case, corresponding to a stronger-than-expected contribution to the EXAFS. These results may arise from the omission of sd interference (see Sec. III). The discrepancies in bond distance are similar in sign and magnitude to shifts observed by Stöhr and Jaeger for the polarized surface EXAFS of Au chemisorbed on Si(111) when the sd interfer-

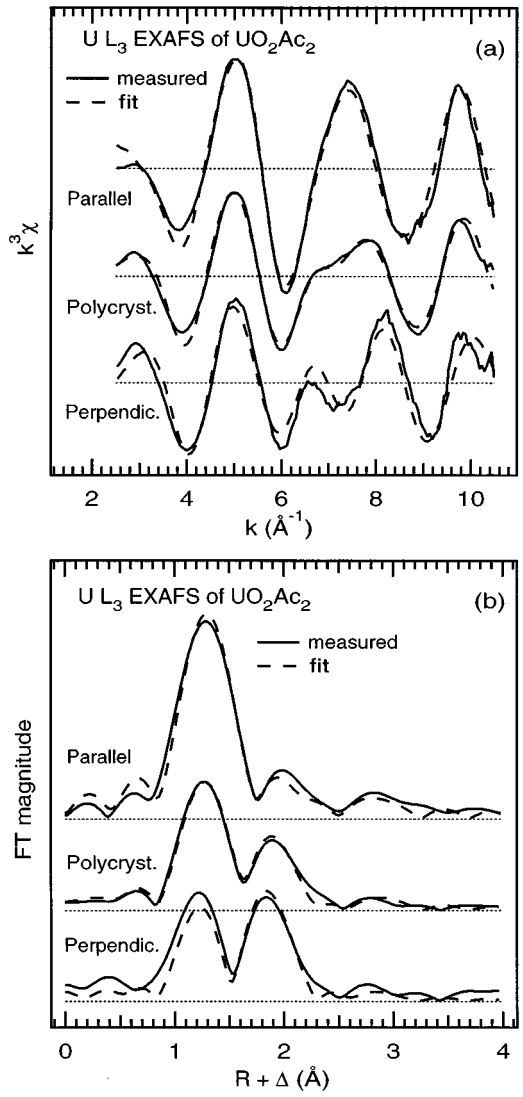

FIG. 4. Polarization dependence for UO_2Ac_2 L_3-edge EXAFS. (a) $k^3\chi$ curves and (b) Fourier transforms of the $k^3\chi$ curves. Note that the FT's do not include phase-shift corrections, so the measured bond distances, as derived from the least-squares analysis, differ from the peak positions plotted here.

ence term was not included in the data analysis.[26] They also found that sd interference caused modifications of the scattering amplitude, which could explain the relatively large axial contribution observed here for perpendicular polarization. The present results support the conclusion of Stöhr and Jaeger that sd interference in the final state should be included for an accurate modeling of polarized L_3-edge EXAFS.

C. Multiple scattering

Based on its polarization dependence and phase-shifted path length, the FT peak at $R+\Delta \approx 2.8$ Å was tentatively attributed above to MS in the axial uranyl bond. For parallel polarization, where this feature is enhanced, a reasonably good fit to this FT feature is obtained based on MS contributions with no adjustable parameters. This is further evidence for the MS origin of this feature.

Because the parallel data set provides this fairly well-isolated MS feature in the FT, it presents an opportunity to study EXAFS MS effects in some detail. In order to extract only the MS contributions in the region of the MS peak, an alternative fit to the parallel EXAFS was performed, in which each of the two SS paths had an additional adjustable parameter E_0. This resulted in a closer fit for the two SS peaks. The MS path was then removed from the calculation, and the residual, i.e., the difference between the calculated and experimental EXAFS, was computed. This residual was Fourier filtered to select contributions within the range $R+\Delta = 2.5$–3.25 Å. The resulting $k^3\chi(k)$ curve, which represents the extracted MS contribution to the EXAFS, is plotted in Fig. 5.

FEFF 6 calculations have been performed to model the extracted MS EXAFS. Three MS paths of the appropriate length are possible due to scattering within the uranyl species, as described in Sec. III. The calculated $k^3\chi(k)$ curves for these paths are shown in Fig. 6, using path lengths and DW factors based on the fit to the axial SS (see Table I, parallel data set). The MS DW factors were obtained from the SS DW factor using the relations derived in Sec. III, with $q=2$ for MS1 and MS3.

It is evident from Fig. 6 that the EXAFS contributions from paths MS2 and MS3 tend to cancel each other for $k<5$ Å, where they might otherwise have more amplitude

TABLE I. Results of fits to UO_2Ac_2 L_3-edge EXAFS. Uncertainties, given in parentheses, are determined by the least-squares minimization and do not reflect possible systematic errors.

Data set	Shell	N^e [a]	R (Å)	σ^2 (Å^2)	R (Å) (from XRD[b])
Parallel	Axial	4.00	1.787 (0.001)	0.002 24 (0.000 13)	
	equatorial	2.50	2.331 (0.005)	0.008 57 (0.000 76)	
Polycrystalline	Axial	2.00	1.768 (0.001)	0.001 52 (0.000 13)	1.751[c]
	equatorial	5.00	2.384 (0.002)	0.011 19 (0.000 33)	2.394[d]
Perpendicular	Axial	1.00	1.717 (0.004)	0.000 05 (0.000 40)	
	equatorial	5.97	2.378 (0.003)	0.008 06 (0.000 43)	

[a]Not varied in fit—calculated from the XRD structure of UO_2Ac_2 using Eq. (2).
[b]Reference 18.
[c]Average of 1.741 and 1.762 Å .
[d]Average of 2.346 Å (1), 2.365 Å (2), 2.447 Å (2), using the weights given in parentheses.

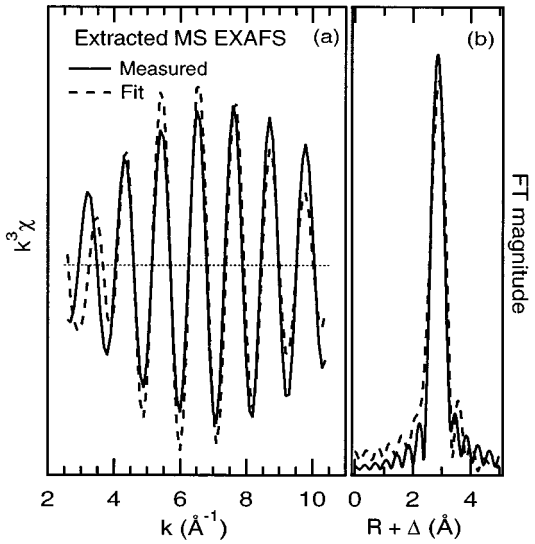

FIG. 5. The multiple-scattering contribution to the UO_2Ac_2 L_3-edge EXAFS; (a) $k^3\chi$ curves, (b) FT's of the $k^3\chi$ curves. The solid lines represent the measured MS contribution, extracted as described in the text. The dashed lines represent a fit based on a single MS path, MS1, with overlap parameter $u=0.0$.

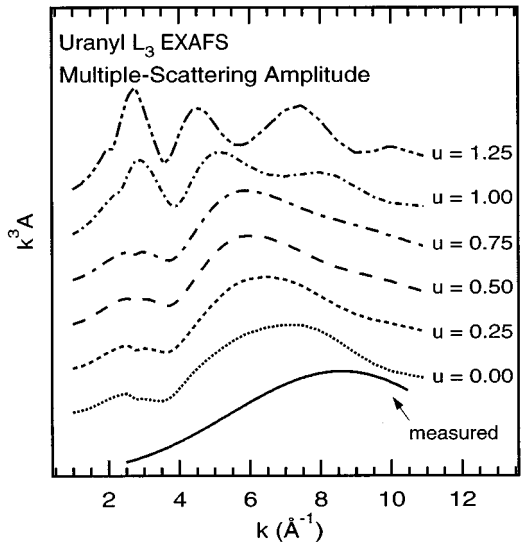

FIG. 7. Comparison of measured and calculated multiple-scattering amplitudes, k^3A. The values of the muffin-tin overlap parameter u are shown for each calculated curve.

than MS1. Furthermore, fits to the extracted MS EXAFS indicate that MS1 yields a much closer match to experiment than either MS2 or MS3, even when the DW factors are varied independently. Apparently a single MS path provides the best model for the MS EXAFS, in contrast to results presented above and in Ref. 15, which indicate that several MS paths are needed to reproduce uranyl XANES resonances. For the fits of Sec. V B, MS1 was the only MS path used. Fits to uranyl EXAFS data for other compounds and complexes also indicated that this path alone is capable of modeling MS effects.[5,6]

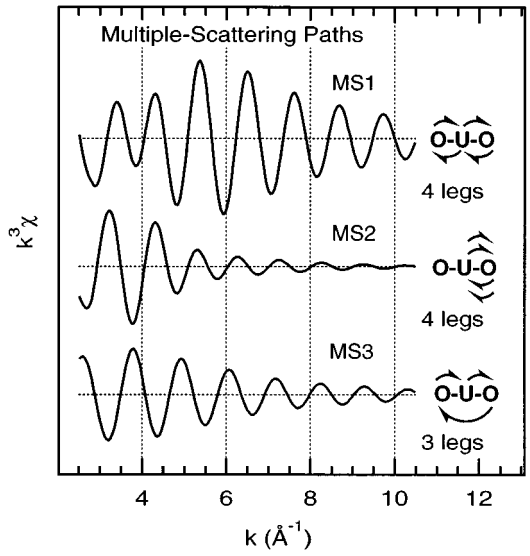

FIG. 6. $k^3\chi$ curves for multiple-scattering paths, calculated using FEFF 6. The paths, labeled MS1, MS2, and MS3, are shown schematically on the right side.

By selecting a path length and coordination number, a scattering amplitude function can be isolated from the extracted MS EXAFS. The result of this treatment is plotted in Fig. 7, based on a path length twice that of the axial SS fit result (parallel data set), and $N^e=4$. Also plotted are calculated FEFF 6 curves k^3A, where

$$A_i(k)=S_0^2C(k)F_i(k,R_i)\exp\left(\frac{-2R_i}{\lambda(k)}\right)\exp(-2\sigma_i^2k^2) \quad (4)$$

is a function which may be compared to the experimentally derived amplitude, and includes backscattering magnitude, DW broadening, and the loss factors from Eq. (1). The curves in Fig. 7 are calculated for the path MS1, using the same DW factor as in Fig. 6. The strong dependence of k^3A upon the muffin-tin overlap parameter, u, defined in Sec. IV B 2, is illustrated in Fig. 7. Most of the observed variation originates in F_i. It is apparent that the best agreement between the calculated and experimentally derived MS EXAFS amplitude is obtained for $u=0.0$, i.e., no overlap. This results contrasts that found for L_1 XANES above, where the best agreement between calculated and measured spectra was obtained using $u=1.0$, i.e., considerable overlap. Overlap was also shown to be important for the L_3 XANES of uranyl fluoride.[15] Figure 5 shows the result of a fit to the extracted MS EXAFS, using the path MS1 calculated with $u=0.0$, where the DW factor was varied. The final MS DW factor is related to the axial SS value by $q=1.50$. The fit is reasonably good, but Figs. 5 and 7 clearly indicate that FEFF 6 is not completely successful in modeling the amplitude of the MS contributions. Note that the calculations shown in Figs. 5–7 do not include the polarization-dependent part of the curved-wave corrections. However this effect was very small for the MS paths, much less than for SS.

VI. CONCLUSIONS

Striking linear dichroism effects have been measured in the uranium L_1- and L_3-edge XANES, and L_3-edge EXAFS,

of uranyl acetate dihydrate. Photoelectron multiple-scattering calculations, using FEFF 6, have been employed to model these effects. The calculated XANES spectra are in good agreement with the measured spectra, especially for the L_1 edge. The success of this one-electron approach suggests that multielectron effects are not important in these spectra. A detailed understanding of the origin of the L_1 XANES is obtained by isolating the scattering paths which contribute to individual spectral features. MS paths within the uranyl cation have a notable influence, in particular by producing a sharp resonance at the L_1 edge jump, which is strongly enhanced when the polarization is parallel to the uranyl axis. Examination of the polarization dependence of the *experimental* L_1 XANES gives substantially the same results as the *theoretical* path analysis of the unpolarized L_1 XANES. This correspondence emphasizes that FEFF 6 calculations provide a valuable tool for the interpretation of measured XANES. Such a theoretical approach is particularly useful for those cases where oriented samples, and thus polarized measurements, are unavailable or impractical.

For polarization parallel to the uranyl species, the L_3 EXAFS shows an FT feature which is attributed to MS within uranyl. This result indicates that any analysis of uranyl EXAFS should include MS contributions to obtain reliable structural information beyond the equatorial shell (i.e., $R > 2.5$ Å .) The scattering amplitude extracted from this MS feature was most successfully modeled by FEFF 6 when the muffin-tin spheres were not overlapped. That contrasts the results of calculations for L_3 XANES, in Ref. 15, and for L_1 XANES, presented here. For both of these edges significant overlapping was found to improve the agreement with experimental XANES. The nonoverlapped potential, which is generally preferable because it is self-consistent, is apparently a better model at higher k, but is less successful at low k. This result highlights the need for an improved treatment of anisotropic bonding within an electron-scattering formalism.

The large polarization dependence of uranyl XANES could be exploited to measure the orientation of this linear species, in the tradition established for molecules on surfaces using soft x-ray absorption.[36] For example, polarized XANES might be used to determine the orientation of adsorbed uranyl relative to a layered mineral substrate. Such structural information would complement that obtained by EXAFS.

ACKNOWLEDGMENTS

We wish to thank D. Templeton, L. Templeton, and D. Perry for advice on the growth and characterization of single crystals, J. Rehr for advice on scattering theory and the use of FEFF 6, and J. Bucher, N. Edelstein, and D. Shuh for assistance in the XAS measurements. This work was supported in part by the Division of Materials Science, Office of Basic Energy Science, and performed under the auspices of the U.S. Department of Energy by Lawrence Livermore National laboratory under Contract No. W-7405-ENG-48. Experimental measurements were made at SSRL, which is operated by the U.S. Department of Energy, Office of Basic Energy Sciences, Divisions of Chemical Sciences and Materials Science.

[1] H. Wanner and I. Forest, *Chemical Thermodynamics of Uranium* (North-Holland, New York, 1992).
[2] R. G. Denning, in *Gmelin Handbook, Uranium* (Springer-Verlag, New York, 1983), Vol. A6, p. 31.
[3] S. Cotton, *Lanthanides and Actinides* (Oxford, New York, 1991).
[4] R. G. Denning, Struct. Bonding (Berlin) **79**, 215 (1992).
[5] P. G. Allen, J. J. Bucher, D. L. Clark, N. M. Edelstein, S. A. Ekberg, J. W. Gohdes, E. A. Hudson, N. Kaltsoyannis, W. W. Lukens, M. P. Neu, P. D. Palmer, T. Reich, D. K. Shuh, C. D. Tait, and B. D. Zwick, Inorg. Chem. **34**, 4797 (1995).
[6] P. G. Allen, D. K. Shuh, J. J. Bucher, N. M. Edelstein, T. Reich, M. A. Denecke, and H. Nitsche, Inorg. Chem. **35**, 784 (1996).
[7] P. Charpin, A. Dejean, G. Folcher, P. Rigny, and P. Navaza, J. Chim. Phys. **82**, 925 (1985).
[8] E. A. Hudson, L. J. Terminello, B. E. Viani, T. Reich, J. J. Bucher, D. K. Shuh, and N. M. Edelstein, in *Applications of Synchrotron Radiation Techniques to Materials Science II*, edited by D. L. Perry, N. D. Shinn, K. L. D'Amico, G. Ice, and L. J. Terminello, MRS Symposia Proceedings No. 375 (Materials Research Society, Pittsburgh, 1995), p. 235.
[9] T. D. Waite, J. A. Davis, T. E. Payne, G. A. Waychunas, and N. Xu, Geochim. Cosmochim. Acta **58**, 5465 (1994).
[10] C. Chisholm-Brause, S. D. Conradson, C. T. Buscher, P. G. Eller, and D. E. Morris, Geochim. Cosmochim. Acta **58**, 3625 (1994).
[11] J.-M. Combes, C. Chisholm-Brause, G. E. Brown, Jr., G. A. Parks, S. D. Conradson, P. G. Eller, I. R. Triay, D. E. Hobart, and A. Meijer, Environ. Sci. Technol. **26**, 376 (1992).
[12] G. E. Brown, Jr., Rev. Mineral. **23**, 309 (1990).
[13] G. Kalkowski, G. Kaindl, W. D. Brewer, and W. Krone, Phys. Rev. B **35**, 2667 (1987).
[14] J. Petiau, G. Calas, D. Petitmaire, A. Bianconi, M. Benfatto, and A. Marcelli, Phys. Rev. B **34**, 7350 (1986).
[15] E. A. Hudson, J. J. Rehr, and J. J. Bucher, Phys. Rev. B **52**, 13 815 (1995).
[16] D. H. Templeton and L. K. Templeton, Acta Crystallogr. A **38**, 62 (1982).
[17] S. I. Zabinsky, J. J. Rehr, A. Ankudoniv, R. C. Albers, and M. J. Eller, Phys. Rev. B **52**, 2995 (1995).
[18] J. Howatson, D. M. Grev, and B. Morosin, J. Inorg. Nucl. Chem. **37**, 1933 (1975).
[19] J. D. H. Donnay and D. Harker, J. Min. Soc. Amer. **22**, 446 (1937).
[20] J. A. Bearden and A. F. Burr, Rev. Mod. Phys. **39**, 125 (1967).
[21] EXAFSPAK was developed by G. George and I. Pickering at SSRL.
[22] J. Mustre de Leon, J. J. Rehr, S. I. Zabinsky, and R. C. Albers, Phys. Rev. B **44**, 4146 (1991).
[23] M. Atoji and M. J. McDermott, Acta Crystallogr. B **26**, 1540 (1970).
[24] S. M. Heald and E. A. Stern, Phys. Rev. B **12**, 5549 (1977).
[25] C. Brouder, J. Phys. Condens. Matter **2**, 701 (1990).
[26] J. Stöhr and R. Jaeger, Phys. Rev. B **27**, 5146 (1983).
[27] C. Brouder, M. F. Ruiz López, R. F. Pettifer, M. Benfatto, and C.

R. Natoli, Phys. Rev. B **39**, 1488 (1989).
[28] M. Benfatto, C. R. Natoli, C. Brouder, R. F. Pettifer, and M. F. Ruiz López, Phys. Rev. B **39**, 1936 (1989).
[29] G. Beni and P. M. Platzman, Phys. Rev. B **14**, 1514 (1976).
[30] J. J. Rehr, R. C. Albers, and S. I. Zabinsky, Phys. Rev. Lett. **69**, 3397 (1992).
[31] M. O. Krause, and J. H. Oliver, J. Phys. Chem. Ref. Data **8**, 329 (1979).
[32] B. Teo and P. A. Lee, J. Amer. Chem. Soc. **101**, 2815 (1979).
[33] N. Rösch, W. G. Klemperer, and K. H. Johnson, Chem. Phys. Lett. **23**, 149 (1973).
[34] J. G. Norman, J. Chem. Phys. **61**, 4630 (1974).
[35] H. A. Thompson, G. E. Brown, Jr., and G. A. Parks, Physica B **208/209**, 167 (1995).
[36] J. Stöhr, *NEXAFS Spectroscopy* (Springer-Verlag, Berlin, 1992).